Fibril Density Reduction in Keratoconic Corneas

Dong Zhou[1], Ahmed Abass[2]*, Bernardo Lopes[2,3], Ashkan Eliasy[2], Sally Hayes[4], Craig

Boote[4], Keith M Meek[4], Alexander Movchan[1], Natalia Movchan[1], Ahmed Elsheikh[2, 5, 6]

[1] Department of Mathematical Sciences, University of Liverpool, Liverpool, UK

[2] School of Engineering, University of Liverpool, Liverpool, UK

[3] Department of Ophthalmology, Federal University of Sao Paulo – Sao Paulo

[4] School of Optometry and Vision Sciences, Cardiff University, Cardiff, UK

[5] Beijing Advanced Innovation Centre for Biomedical Engineering, Beihang University, Beijing,

100083, China

[6] NIHR Biomedical Research Centre for Ophthalmology, Moorfields Eye Hospital NHS

Foundation Trust and UCL Institute of Ophthalmology, London, UK

*Corresponding author: Dr Ahmed Abass, School of Engineering, University of Liverpool,

Liverpool, UK, a.abass@liverpool.ac.uk

Keywords: cornea; keratoconus; tissue microstructure; ocular biomechanics

Word count: 5279

Abstract

This study aims to estimate the reduction in collagen fibril density within the central 6mm radius of keratoconic corneas through processing of microstructure and videokeratography data. Collagen fibril distribution maps and topography maps were obtained for seven keratoconic and six healthy corneas, and topographic features were assessed to detect and calculate the area of the cone in each keratoconic eye. The reduction in collagen fibril density within the cone area was estimated with reference to the same region in the characteristic collagen fibril maps of healthy corneas. Together with minimum thickness and mean central corneal refractive power, the cone area was correlated with the reduction in the cone collagen fibrils. For the corneas considered, the mean area of keratoconic cones was 3.30 ± 1.90 mm^2. Compared with healthy corneas, fibril density in the cones of keratoconic corneas was lower by as much as 35% and the mean reduction was 17±10%. A linear approximation was developed to relate the magnitude of reduction to the refractive power, minimum corneal thickness and cone area (R^2= 0.95, p< 0.001). Outside the cone area, there was no significant difference between fibril arrangement in healthy and keratoconic corneas. The presented method can predict the mean fibril density in the keratoconic eye's cone area. The technique can be applied in microstructure-based finite element models of the eye to regulate its stiffness level and the stiffness distribution within the areas affected by keratoconus.

Introduction

Keratoconus (KC) is a bilateral non-inflammatory corneal disease that affects approximately 1 in 2000 of the population (1). The keratoconic cornea progressively develops ectasia with local thinning and a cone-shaped protrusion, which results in visual impairment. The management of KC, including its diagnosis and treatment, has developed significantly in recent decades.

Computer-assisted videokeratography provides quantitative imaging of corneal anterior and posterior topographies. KC can be detected and classified based on corneal topography through clinical signs of disease evolution, index-based classification systems and advanced machine learning algorithms (1-7). These detection techniques are clinically useful to evaluate the stage of KC and guide the selection of suitable treatments.

Corneal shape is the outcome of an equilibrium between the intraocular pressure (IOP) and the mechanical resistance (or stiffness) of ocular tissue. In keratoconic eyes, and in particular within the KC cone, the stiffness of corneal tissue is known to be lower than in healthy corneas due to the combined effect of smaller thickness and softer material (8-12). The reduced stiffness in the cone is thought to be the cause of the distortion of the tissue and the subsequent loss in vision clarity.

While the pathogenesis of KC remains unclear, there is strong evidence that the microstructural alterations in cone tissue, in terms of both collagen fibril density and organisation, are behind the reduced stiffness of KC tissue. Literature in this field shows consistently that healthy corneas have preferential fibril organisation with more fibrils lying in the horizontal and vertical directions than in any other direction in the central region of the cornea; the fibrils then gradually assume an increasingly tangential arrangement with increasing proximity to the limbus (13-15). This arrangement is clearly disturbed in KC eyes and is accompanied by a significant reduction in fibril content (16-18), and a decreased incidence of collagen interlacing between lamellae in the para-apical region (19, 20). These changes cause loss of mechanical cohesiveness, and facilitate slippage between stromal

72 lamellae (16, 21). Hayes, Boote (18) demonstrated that these effects were concentrated in the

73 area where the KC cone develops with significant local thinning and surface distortion, thus

74 providing evidence of an association between microstructural degradation and topographical

75 distortion.

76 The last two decades saw several attempts to develop numerical models of ocular

77 biomechanical behaviour based on the tissue's microstructure and in particular its collagen

78 fibril distribution. These models benefitted from the extensive work carried out in X-ray

79 scattering studies to quantify the fibril density and orientation across the cornea (22-26).

80 However, while similar studies have attempted to quantify the microstructural features of KC

81 corneas, no consensus has developed yet on the effect of KC on fibril organisation.

82 This study attempts to address this shortfall through analysis of microstructure maps of seven

83 KC corneas and six healthy corneas. It seeks to provide an estimate of the reduction in fibril

84 density within the cone area that can be expected in eyes with different disease severity stages,

85 thickness loss and cone surface areas. With this information, progress can be made in building

86 patient-specific, microstructure-based numerical models of the biomechanical behaviour of

87 KC eyes.

88

Methods
89

Collagen fibril maps
90

91 This study utilised a large collection of previously published x-ray scattering data that was

92 gathered for a number of individual studies (15, 27-29), and done so in accordance with the

93 ethical principles of the declaration of Helsinki and its subsequent revisions, with full, informed

94 consent from the human tissue donors, and with approval from the Human Science Ethical

95 Committee (School of Optometry and Vision Sciences, Cardiff University, UK). This study

96 involved 6 healthy donor corneas (with at least 13 mm of surrounding sclera), collected post-

97 mortem from 4 donors aged between 54 and 75 years. It also included 7 central corneal

98 buttons with severe keratoconus (KC) collected using 7.5 mm diameter trephines from 7

99 donors aged between 24 and 39 years who underwent penetrating keratoplasty. The patients'

100 demographic characteristics and corneal thickness values are summarised in Table 1.

101

102 Table 1 Patients' demographic characteristics including age, gender, left/right eyes.

	Healthy	Keratoconus	
Number of corneas and donors	6, 4	7, 7	
Age in years (mean±SD range)	65.0±8.8 (54 – 75)	30.1±4.4 (24 – 39)	p < 0.001
Left:Right eyes ratio	1.0:1.0	1.0:2.5	p = 0.576
Male:Female gender ratio	1:1	1:1.3	p = 1.000
Central corneal thickness (mean±std μm)	546.4±12.5	293.7±88.2	p < 0.001

103

104

105 The healthy corneas were obtained within 18 hrs post-mortem, stored at 4°C for transport and

106 subsequently fixed in 4% PFA prior to scanning by wide-angle x-ray scattering (WAXS), while

107 the KC corneas were obtained post-operatively, quickly frozen in liquid Nitrogen and stored at

108 -80ºC until required for data collection. This difference in tissue preparation methods was

109 found earlier to have no significant effect on WAXS data (30).

110 Thickness measurements were taken in healthy eyes prior to PFA tissue fixation using an

111 ultrasound pachymeter (Pachmate 55; DGH Technologies, Exton, PA) with ±5 µm accuracy

112 (Table 1). The thickness was measured at the centre of each cornea and at intervals of 2.5

113 mm along 8 meridians. Measurements were taken 3 times at each point and the mean value

114 was used. Recorded standard deviation was less than 10 µm for all pachymetry thickness

115 measurements. Interpolation between these values was then used to estimate the tissue

116 thickness throughout the corneal surface. On the other hand, the thickness across the surface

117 of keratoconic corneas was obtained directly from the videokeratography images recorded

118 prior to the penetrating keratoplasty (Table 1). The different methods used to measure the

119 thickness were found in the past to produce similar results, and were therefore not expected

120 to make a notable effect on the results of this study (31, 32).

121 Based on the measured central corneal thickness of the healthy specimens (530-560 µm) and

122 the known relationship between thickness and hydration, the healthy corneas were deemed

Due to the large dimensions of the healthy cornea-scleral specimens relative to the size of the

specimen holder, it was necessary to flatten the tissue slightly prior to scanning. This was

achieved by performing a series of six meridional incisions, extending from the corneal limbus

to the outer edge of the sclera (thus avoiding damage to the cornea itself) (15, 27).

Just before testing, the KC corneas were thawed, and both the healthy and KC tissue was

wrapped in polyvinylidene chloride catering film to minimise tissue dehydration. Wide angle x-

rays scatter (WAXS) patterns were obtained from each specimen in a grid system of 0.5 mm

intervals in both horizontal and vertical directions for healthy eyes (27), and 0.25 mm intervals

for KC eyes (29). The x-ray scattering images collected at every scanning spot were

normalised against the x-ray beam intensity and the x-ray exposure time, and subsequently

analysed to determine the orientation of fibrillar collagen at equally-spaced 256 orientations

covering 360°, as well as the total collagen x-ray scatter intensity at each sampling position.

150   Due to the potential for tissue distortion artefacts close to the cut edges in both the healthy

151   and keratoconus specimens, data obtained within 0.75 mm of the sample edge was excluded

152   from the analysis.

153

154   **Identification of cone area in KC corneas**

155   Videokeratography scans of the keratoconic buttons were obtained using Orbscan (Bausch &

156   Lomb, Technolas PV, Germany) before the surgery, in which they were removed. These scans

157   provided corneal anterior and posterior topography maps, mean power maps and thickness

158   distribution maps. Central corneal thickness measurements with partial coherence

159   interferometry, ultrasound, and the Orbscan system (33). The topography maps enabled

160   calculation of the height of the cornea relative to a best-fit spherical surface, with the highest

161   point assumed to represent the centre of the keratoconic cone (34, 35). The refractive power

162   P was calculated using the Gaussian optics formula (36-38).

$$P = \frac{n_{cornea} - n_{air}}{R_{anterior}} + \frac{n_{aqueous} - n_{cornea}}{R_{posterior}} - \frac{t_c}{n_{cornea}} \times \frac{n_{cornea} - n_{air}}{R_{anterior}} \times \frac{n_{aqueous} - n_{cornea}}{R_{posterior}} \tag{1}$$

163   Where the refractive indices of air, n_{air}, cornea, n_{cornea}, and aqueous, $n_{aqueous}$, were set at

164   1.0, 1.376 and 1.336, respectively following Gullstrand's relaxed eye model (39, 40), and t_c,

165   represented the central corneal thickness. The sagittal radii of curvatures at any point were

166   calculated as:

$$R = \frac{x}{\cos\left(\frac{\pi}{2} - \alpha\right)} \tag{2}$$

167   where α is the tangent angle at the calculation point and x is the distance from the apex.

168   The mean power map was constructed based on the average of the two principal curvatures

169   at each scanned point (38).

170

171   The boundary of keratoconic cones was detected based on the observation that it coincided

172   with a sudden, abnormal reversal of corneal curvature. As outlined in our earlier studies (35,

173   41, 42), corneal profiles along equally-spaced meridian lines originating at the cone centre

174 and extending outwards were analysed. Initially, a sphere was fitted to the central, 8 mm

175 diameter area of each corneal anterior surface, and the radial distance from each data point

176 on a corneal surface to the centre of the sphere was calculated. This was followed by

177 subtracting the radius of the sphere from these radial distances and the position and

178 magnitude of the largest positive difference were assumed to point at the location and height

179 of the cone centre, respectively.

180 To estimate the area of pathology, height data relative to the optimal sphere were determined

181 along 360 equally-spaced lines meeting at the cone centre and extending outwards using

182 triangle-based cubic interpolation (43). A first derivative of the height data was calculated to

183 determine the tangent to the surface along these lines. The second derivative was then

184 calculated to represent the rate of change of this gradient. Since the rate of gradient change

185 experiences a change in direction when the point of interest moves from the cone area to the

186 surrounding healthy area, a sudden change in the sign of the rate of change in tangent

187 gradient is indicative of an intersection with the transition zone between the pathologic area

188 and the remaining corneal tissue. Locating the transition zone between the area of pathology

189 and the remaining corneal tissue using this method then allowed calculating the cone area.

190 An iterative process was then initiated in which the cone area was removed from the

191 topography data before re-identifying the optimal sphere and repeating the subsequent steps.

192 This process was repeated until the difference between the results (cone height and centre

193 location) of two subsequent analyses became smaller than 1.0 μm.

194

195 **Fibril density reduction factor 'κ'**

196 Assessment of the reduction in collagen fibril density in KC cones started with developing a

197 map representing the mean density distribution in the six healthy corneas scanned. As it was

198 not possible to scan at exactly the same points in all cornea specimens, as discussed in our

199 previous study Zhou, Eliasy (15), 10th order Zernike polynomials were used to fit the fibril

density measurements obtained for each cornea. The average values of Zernike coefficients were then determined and used to represent the mean density distribution for healthy corneas. This process enabled comparison of fibril density in KC corneas (both within and outside cone boundary) with mean fibril density in the corresponding areas of healthy corneas. Therefore, the analysis included two sets of comparisons. First, the fibril density within the cone area in keratoconic corneas was compared to the density in corresponding areas in healthy corneas. The second comparison was between the fibril density outside the cone in keratoconic corneas and the density in corresponding areas in healthy eyes. This exercise led to the development of a fibril density reduction factor (κ) that quantified the mean reduction in fibril density in each KC cone relative to the corresponding area in healthy corneas:

$$\kappa = \frac{C_k}{C_h}\frac{S_h}{S_k} \tag{3}$$

where, for each KC cone, C_h and S_h are the mean fibril density in the healthy corneal areas that correspond to the areas inside (C) and outside (S) the KC cone, respectively. Likewise, C_k and S_k represent the mean fibril density inside and outside the cone area in each KC cornea. Expressing the fibril reduction factor as a ratio was used to eliminate any hydration-induced variation in absolute collagen scatter caused by the different sample storage methods of KC and healthy corneal specimens.

A stepwise linear regression model was fitted to assess the correlation between κ and topographic features of the cornea including the mean central refractive power (P) obtained within the central 3mm diameter zone, the minimum corneal thickness (T), the KC cone area (A) and the distance between the cone centre and corneal apex (D). Both P and T were extracted from the Obscan reports. Using the forward stepwise approach, the variables that could explain most of the variance in κ and therefore composed the final model were P, T and A.

The first-order polynomial adopted for the dependence of κ on P, T and A took the following form (the first order was adopted to avoid overfitting, which can be caused by the small size of the database):

$$\kappa = a_1 A + a_2 P + a_3 T + a_4 \qquad (4)$$

226 In Equation 4, a_1 to a_4 are constants, which were optimised using the least square method

227 with the objective function:

$$\mathrm{RMS} = \frac{1}{n} \sum_{i=1}^{n} \left(\kappa_{mi} - \kappa_e(A_i, P_i, T_i) \right)^2 \qquad (5)$$

228 Where RMS is the root mean square error, n is the number of data points, κ_{mi} is the measured

229 value of density reduction based on KC fibril map i, and κ_e is the estimated density reduction

230 based on Equation 4. Each KC cornea provided one data point i, and six more points were

231 added to represent the healthy corneas, with $\kappa = 1$, $A = 0$, $P \in [43D, 45D]$, $T \in$

232 $[530\mu m, 560\mu m]$.

233 K-fold cross-validation was used to test the accuracy of the linear model in predicting fibril

234 density reduction. Data of one keratoconic cornea was kept in every validation cycle to be

235 used in testing the regression model, while data of other eyes were used in its training and

236 calculating its coefficients. The model finally adopted the average values of coefficients

237 following all K-fold cross-validation steps.

Statistical analysis

239 Statistical analysis was carried out using the MATLAB and Statistics Toolbox Release 2019b

240 (The MathWorks, Inc., Natick, Massachusetts, United States). The Goodness-of-fit of the

241 regression model relating κ to P, T and A was evaluated with the coefficient of determination

242 (R^2). The closer the R^2 is to 1, the higher the variation of the dependent variable explained by

243 the independent variables in the regression model. The comparison of the continuous

244 variables was performed using either Student's t-test or Mann-Whitney U-test according to the

245 variables' distribution. The categorical variables were compared using the Chi-Squared test.

246 A p-value lower than 0.050 was considered statistically significant.

247

Results

KC cone area

Figure 1 shows the fibril density maps of the seven keratoconic corneas with the estimated cone boundary marked in each case. The cone area (A), the central refractive power (P), the minimum thickness (T), and the fibril reduction factor (κ) measured from the fibril density maps are also listed in Table 2. The results show trends in which increases in cone area or mean power, or decreases in min thickness were associated with higher fibril density reductions (i.e. smaller κ). However, despite the significant correlation between κ and each of A, P and T, there was no correlation between A and P (p= 0.37), A and T (p= 0.89), or R and T (p= 0.18).

(a) KC1, Left	(b) KC2, Right	(c) KC3, Right

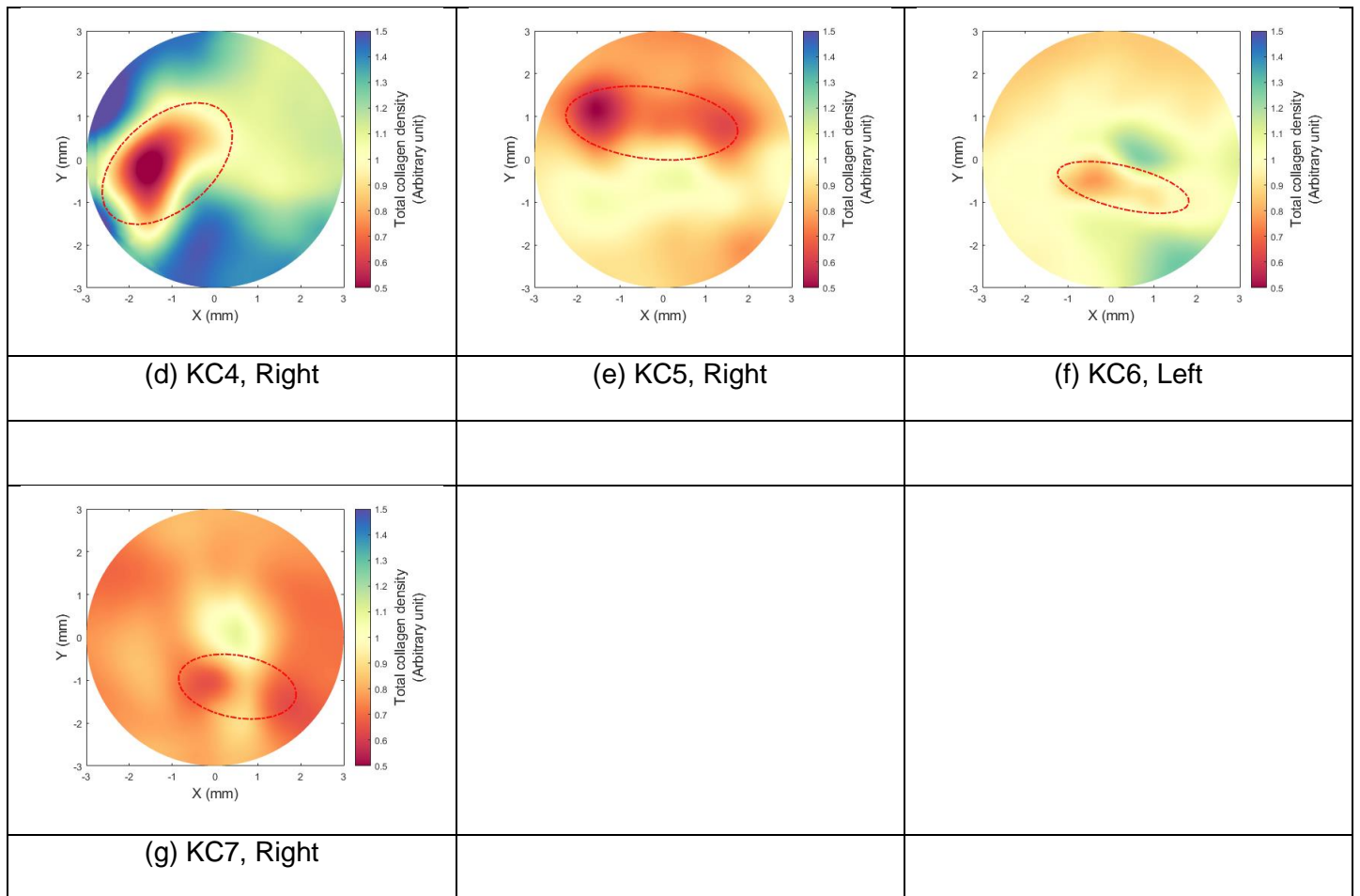|		
(d) KC4, Right	(e) KC5, Right	(f) KC6, Left
(g) KC7, Right		
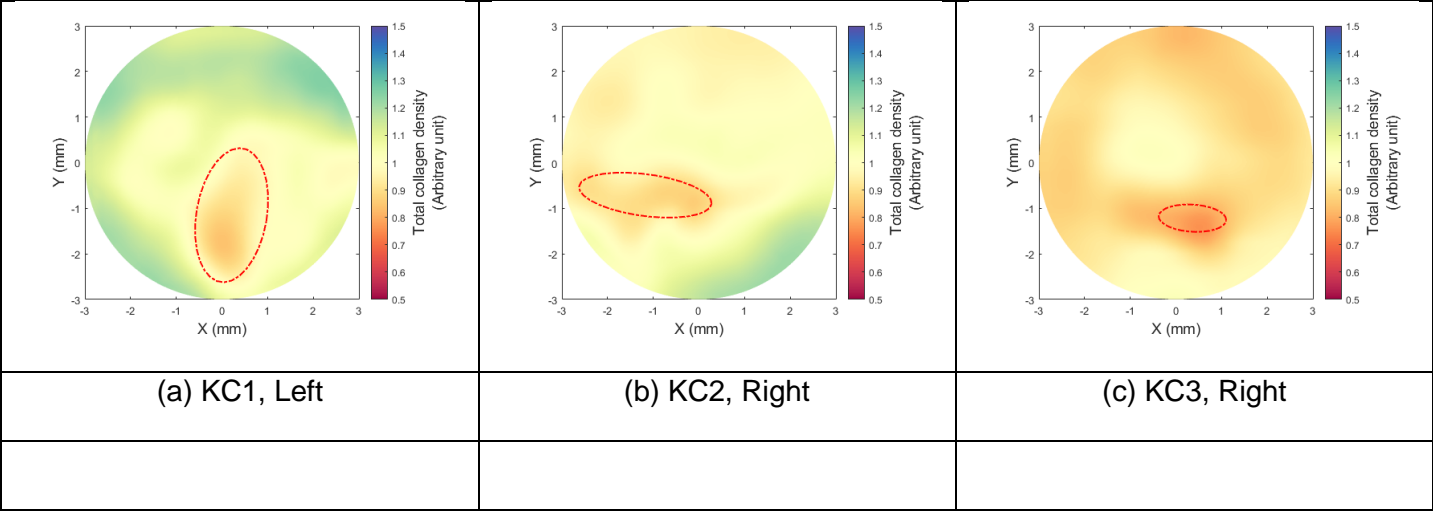
Figure 1 Fibril density maps for seven keratoconic corneas. S, I, T and N indicate superior, inferior, temporal and nasal directions, respectively. The origin (0,0) is the corneal apex. Red lines represent the KC cone boundaries.

Table 2 Measurements of cone area, mean central refractive power, minimum thickness and cone fibril density reduction in keratoconic corneas

Specimen	Cone area, A (mm^2)	Mean power, P (Diopter)	Min Thickness, T (μm)	Fibril reduction factor, κ
KC1	3.61	46.90	483.0	0.84
KC2	2.18	49.20	220.0	0.90
KC3	0.72	54.30	298.0	0.91
KC4	6.24	58.30	277.0	0.65
KC5	5.17	59.30	279.0	0.73
KC6	2.07	63.20	227.0	0.89
KC7	3.12	63.20	272.0	0.87
Mean±SD	3.30±1.90	56.34±6.47	293.7±88.2	0.83±0.10

| (min-max) | (0.72-6.24) | (46.90-63.20) | (220.0-483.0) | (0.65-0.91) |

272

273

Fibril distribution comparisons

The effect of KC on fibril distribution outside the cone area was studied with reference to the results in Figure 2. In this figure, the proportion of collagen fibrils in the 45° sectors surrounding the horizontal and vertical directions, and the tangential direction to the cornea edge was quantified within successive tissue rings, each with 0.5 mm width. All the x-ray scanning points in the healthy cornea maps were included in the calculations while the cone areas were excluded from the KC cornea calculations. The results covered the central zones with 3 mm radius in KC corneas and 6 mm radius in healthy corneas.

The central corneas within 3 mm radius had percentages of horizontal and vertical fibril contents between 30% and 35% of total density in both healthy and KC eyes. No significant differences were found in percentages of preferentially aligned horizontal fibrils (p= 0.29) or vertical fibrils (p= 0.22) between healthy and KC corneas. Similarly, there were no significant differences between healthy and KC corneas in the percentages of tangential fibrils – mean values ranged between 24 and 28% in both specimen groups.
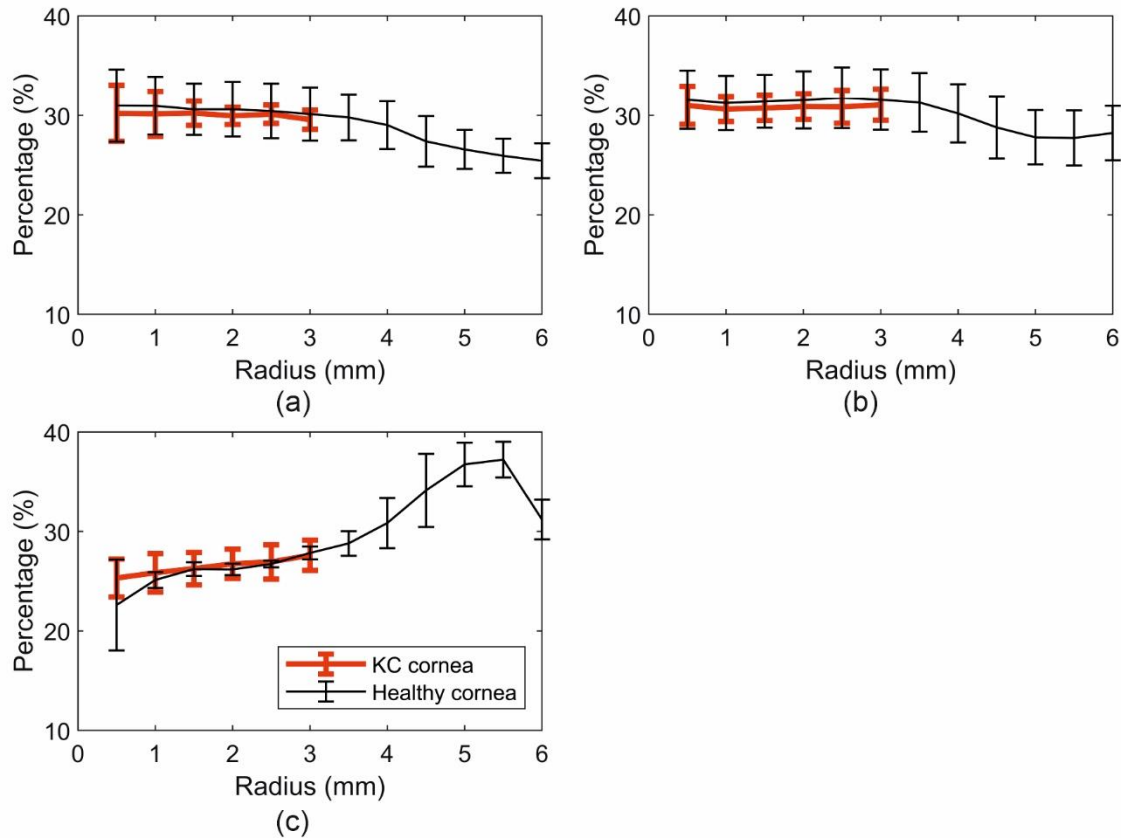
288

Figure 2 Percentage of fibril quantity in (a) the horizontal direction, (b) the vertical direction, and (c) the tangential direction in healthy and keratoconic cornea specimens.

Fibril density reduction factor 'κ'

Values of constants a_1 to a_4 in the linear relationship between κ and A, P and T, were determined using the least square method as:

$$\kappa = -0.0425A - 0.0004P + 0.0001T + 0.9727 \tag{6}$$

The relationship reflected a decrease in κ (denoting a larger fibril density reduction) with lower minimum corneal thickness (T) (p=0.015), larger central refractive power (P) (p=0.003) and larger cone area (A) (p<0.001). The R^2-value was 0.95 (p< 0.001) and indicated the strong fit of Equation 6 to the measured fibril density measurements. The K-fold cross-validation showed 2.00% error in average fibril reduction in training the model and 2.58% in its testing.

14

Discussion

Microstructural abnormality in the KC cornea including irregular fibril arrangement, reduced fibril density, lamellae splitting and decreased lamella interweaving was observed in previous studies (16-18, 21, 44). These microstructural changes lead to deterioration in mechanical stiffness compared with the levels expected in healthy corneas (11, 45). The evident association between the reduced fibril density and the stiffness deterioration has enabled the development of numerical models of KC corneas that consider changes in fibril arrangement (22, 23, 25, 26, 28). However, what remains lacking are methods to estimate reductions in fibril density in individual eyes, which would be needed in construction of customised numerical models of KC corneas. This study seeks to address this gap through developing a relationship between fibril density reduction within the cone and a number of corneal features including the cone area, the mean refractive power and the minimum corneal thickness. The study also attempts to establish the effect of keratoconus on the density and distribution of collagen fibrils outside the cone.

The study started with analysis of microstructure maps of 6 healthy corneas and showed that the collagen fibril distribution was consistent with primarily (30.2±2.8%) of vertical fibrils and (31.5±2.9%) of horizontal fibrils in the central region (up to 3 mm radius). Beyond this region, the fibrils gradually change orientation, becoming more tangentially aligned with respect to the edge of the cornea until the limbus (radius ≈ 5.5 mm) where the percentage of tangential fibrils reaches 37.2±1.8%. Although comparative data was not available from the limbal region of the KC corneas, it was noted that the fibril distribution outside the cone areas was similar to that observed in healthy corneas. In KC corneas, the percentages of the vertical and horizontal fibrils in the central corneas, but excluding the cone areas, were 30.8±1.5% and 30.0±1.5%, respectively, with no significant differences compared to corresponding values in healthy corneas (p= 0.22, 0.29).

The range of fibril density reduction in the cone areas of the 7 KC corneas analysed in this study was between 20 and 39%. This magnitude of density loss was correlated with three

parameters; namely the cone area, the mean refractive power and the minimum corneal thickness (p= 0.001, 0.008, 0.041, respectively). Another parameter, the distance between corneal apex and cone centre, was excluded due to lack of significant correlation with density reduction. Based on these results, an estimate of a cone fibril reduction factor κ was developed and found to offer a close match with measured values. With the proven dependence of corneal stiffness on collagen fibril distribution, this parameter could be employed in numerical analyses to simulate the effect of KC on corneal biomechanical behaviour.

The study has a number of limitations. First, the change in fibril alignment within the cones that has been observed in some keratoconic maps was not consistent and could not be quantified, and therefore could not be considered in the current study. Second, the number of cornea specimens included in the study was relatively small due to the difficulty in obtaining full tissue thickness KC buttons. As new data becomes available, the method developed in this study will be updated.

In conclusion, this study presented a method to estimate the reduction in collagen fibril density inside the cone areas of KC corneas. The study also presented evidence that the fibril distribution outside the cone areas was not affected by KC development and progression and was therefore similar to the fibril distribution in healthy corneas. These findings would make it possible to develop customised numerical models that predict the biomechanical behaviour of KC corneas.

Author Contributions Statement

DZ, BL and AA developed the method and drafted the paper. DZ and AEliasy performed the analysis. BL contributed to the statistical analysis. SH, KM and CB collected the x-ray scattering data. AA, AM, NM and AElsheikh supervised the project. AElsheikh designed the study. All authors reviewed the manuscript.

Acknowledgements

Conflict of Interest Statement

There is no conflict of interest to declare.

References:

1.   Auffarth GU, Wang L, Völcker HE. Keratoconus evaluation using the Orbscan topography system. Journal of Cataract & Refractive Surgery. 2000;26(2):222-8.
2.   Montalbán R, Alio JL, Javaloy J, Piñero DP. Comparative analysis of the relationship between anterior and posterior corneal shape analyzed by Scheimpflug photography in normal and keratoconus eyes. Graefe's Archive for Clinical and Experimental Ophthalmology. 2013;251(6):1547-55.
3.   Tomidokoro A, Oshika T, Amano S, Higaki S, Maeda N, Miyata K. Changes in anterior and posterior corneal curvatures in keratoconus. Ophthalmology. 2000;107(7):1328-32.
4.   Alió JL, Shabayek MH. Corneal higher order aberrations: a method to grade keratoconus. Journal of Refractive Surgery. 2006;22(6):539-45.
5.   Accardo PA, Pensiero S. Neural network-based system for early keratoconus detection from corneal topography. Journal of biomedical informatics. 2002;35(3):151-9.
6.   Yousefi S, Yousefi E, Takahashi H, Hayashi T, Tampo H, Inoda S, et al. Keratoconus severity identification using unsupervised machine learning. PLoS One. 2018;13(11):e0205998.
7.   Krumeich JH, Daniel J. Lebend-Epikeratophakie und Tiefe Lamelläre Keratoplastik zur Stadiengerechten chirurgischen Behandlung des Keratokonus (KK) I-III. Klinische Monatsblätter für Augenheilkunde. 1997;211(08):94-100.
8.   Andreassen TT, Hjorth Simonsen A, Oxlund H. Biomechanical properties of keratoconus and normal corneas. Experimental Eye Research. 1980;31(4):435-41.
9.   Scarcelli G, Besner S, Pineda R, Yun SH. Biomechanical Characterization of Keratoconus Corneas Ex Vivo With Brillouin MicroscopyEvaluation of Brillouin Microscopy for Keratoconus. Investigative Ophthalmology & Visual Science. 2014;55(7):4490-5.
10.   Reinstein DZ, Gobbe M, Archer TJ, Silverman RH, Coleman DJ. Epithelial, stromal, and total corneal thickness in keratoconus: three-dimensional display with artemis very-high frequency digital ultrasound. Journal of Refractive Surgery. 2010;26(4):259-71.
11.   Mikula E, Winkler M, Juhasz T, Brown DJ, Shoa G, Tran S, et al. Axial mechanical and structural characterization of keratoconus corneas. Experimental Eye Research. 2018;175:14-9.
12.   Nash IS, Greene PR, Foster CS. Comparison of mechanical properties of keratoconus and normal corneas. Experimental eye research. 1982;35(5):413-24.
13.   Aghamohammadzadeh H, Newton RH, Meek KM. X-Ray Scattering Used to Map the Preferred Collagen Orientation in the Human Cornea and Limbus. Structure. 2004;12(2):249-56.
14.   Meek K. The cornea and sclera. Collagen: structure and mechanics. 2008:359-96.

398   15.   Zhou D, Eliasy A, Abass A, Markov P, Whitford C, Boote C, et al. Analysis of X-ray scattering
399   microstructure data for implementation in numerical simulations of ocular biomechanical behaviour.
400   PLOS ONE. 2019;14(4):e0214770.
401   16.   Daxer A, Fratzl P. Collagen fibril orientation in the human corneal stroma and its implication
402   in keratoconus. Investigative ophthalmology & visual science. 1997;38(1):121-9.
403   17.   Meek KM, Tuft SJ, Huang Y, Gill PS, Hayes S, Newton RH, et al. Changes in collagen
404   orientation and distribution in keratoconus corneas. Investigative ophthalmology & visual science.
405   2005;46(6):1948-56.
406   18.   Hayes S, Boote C, Tuft SJ, Quantock AJ, Meek KM. A study of corneal thickness, shape and
407   collagen organisation in keratoconus using videokeratography and X-ray scattering techniques.
408   Experimental Eye Research. 2007;84(3):423-34.
409   19.   Radner W, Zehetmayer M, Skorpik C, Mallinger R. Altered organization of collagen in the
410   apex of keratoconus corneas. Ophthalmic research. 1998;30(5):327-32.
411   20.   Morishige N, Wahlert AJ, Kenney MC, Brown DJ, Kawamoto K, Chikama T-i, et al. Second-
412   Harmonic Imaging Microscopy of Normal Human and Keratoconus Cornea. Investigative
413   Ophthalmology & Visual Science. 2007;48(3):1087-94.
414   21.   Dawson DG, Randleman JB, Grossniklaus HE, O'Brien TP, Dubovy SR, Schmack I, et al. Corneal
415   Ectasia After Excimer Laser Keratorefractive Surgery: Histopathology, Ultrastructure, and
416   Pathophysiology. Ophthalmology. 2008;115(12):2181-91.e1.
417   22.   Pinsky PM, van der Heide D, Chernyak D. Computational modeling of mechanical anisotropy
418   in the cornea and sclera. Journal of Cataract \& Refractive Surgery. 2005;31(1):136-45.
419   23.   Studer H, Larrea X, Riedwyl H, Büchler P. Biomechanical model of human cornea based on
420   stromal microstructure. Journal of biomechanics. 2010;43(5):836-42.
421   24.   Pandolfi A, Manganiello F. A model for the human cornea: constitutive formulation and
422   numerical analysis. Biomechanics and modeling in mechanobiology. 2006;5(4):237-46.
423   25.   Pandolfi A, Holzapfel GA. Three-dimensional modeling and computational analysis of the
424   human cornea considering distributed collagen fibril orientations. Journal of biomechanical
425   engineering. 2008;130(6):061006.
426   26.   Whitford C, Studer H, Boote C, Meek KM, Elsheikh A. Biomechanical model of the human
427   cornea: Considering shear stiffness and regional variation of collagen anisotropy and density. Journal
428   of the mechanical behavior of biomedical materials. 2015;42:76-87.
429   27.   Pijanka JK, Abass A, Sorensen T, Elsheikh A, Boote C. A wide-angle X-ray fibre diffraction
430   method for quantifying collagen orientation across large tissue areas: application to the human
431   eyeball coat. Journal of Applied Crystallography. 2013;46(5):1481-9.
432   28.   Zhou D, Abass A, Eliasy A, Studer HP, Movchan A, Movchan N, et al. Microstructure-based
433   numerical simulation of the mechanical behaviour of ocular tissue. Journal of The Royal Society
434   Interface. 2019;16(154):20180685.
435   29.   Hayes S, Boote C, Tuft SJ, Quantock AJ, Meek KM. A study of corneal thickness, shape and
436   collagen organisation in keratoconus using videokeratography and X-ray scattering techniques.
437   Experimental Eye Research Journal. 2007;84(3):423-34.
438   30.   Boote C, Dennis S, Huang Y, Quantock AJ, Meek KM. Lamellar orientation in human cornea in
439   relation to mechanical properties. J Struct Biol. 2005;149(1):1-6.
440   31.   Sadoughi MM, Einollahi B, Einollahi N, Rezaei J, Roshandel D, Feizi S. Measurement of central
441   corneal thickness using ultrasound pachymetry and Orbscan II in normal eyes. Journal of ophthalmic
442   & vision research. 2015;10(1):4.
443   32.   Rainer G, Findl O, Petternel V, Kiss B, Drexler W, Skorpik C, et al. Central corneal thickness
444   measurements with partial coherence interferometry, ultrasound, and the Orbscan system.
445   Ophthalmology. 2004;111(5):875-9.
446   33.   Dutta D, Rao HL, Addepalli UK, Vaddavalli PK. Corneal thickness in keratoconus: comparing
447   optical, ultrasound, and optical coherence tomography pachymetry. Ophthalmology.
448   2013;120(3):457-63.

449   34.   Mahmoud AM, Roberts CJ, Lembach RG, Twa MD, Herderick EE, McMahon TT. CLMI: the
450   cone location and magnitude index. Cornea. 2008;27(4):480-7.
451   35.   Eliasy A, Abass A, Lopes BT, Vinciguerra R, Zhang H, Vinciguerra P, et al. Characterization of
452   cone size and centre in keratoconic corneas. Journal of The Royal Society Interface.
453   2020;17(169):20200271.
454   36.   Olsen T. On the calculation of power from curvature of the cornea. The British Journal of
455   Ophthalmology. 1986;70(2):152-4.
456   37.   Ho J-D, Tsai C-Y, Tsai RJ-F, Kuo L-L, Tsai IL, Liou S-W. Validity of the keratometric index:
457   Evaluation by the Pentacam rotating Scheimpflug camera. Journal of Cataract & Refractive Surgery.
458   2008;34:137-45.
459   38.   Abass A, Clamp J, Bao F, Ambrosio R, Jr., Elsheikh A. Non-Orthogonal Corneal Astigmatism
460   among Normal and Keratoconic Brazilian and Chinese populations. Curr Eye Res. 2018:1-8.
461   39.   Smit G, Atchison DA. The eye and visual optical instruments: Cambridge University Press;
462   1970.
463   40.   Vojnikovi Bo, Tamajo E. Gullstrand's Optical Schematic System of the Eye Modified by
464   Vojnikovi & Tamajo. Coll Antropol. 2013;37 (1):41-5.
465   41.   Abass A, Lopes BT, Eliasy A, Wu R, Jones S, Clamp J, et al. Three-dimensional non-parametric
466   method for limbus detection. PLOS ONE. 2018;13(11):e0207710.
467   42.   Abass A, Lopes BT, Eliasy A, Salomao M, Wu R, White L, et al. Artefact-free topography based
468   scleral-asymmetry. PLOS ONE. 2019;14(7):e0219789.
469   43.   Renka RJ, Renka RL, Cline AK. A TRIANGLE-BASED C^1 INTERPOLATION METHOD. The Rocky
470   Mountain Journal of Mathematics. 1984;14(1):223-37.
471   44.   Mathew JH, Goosey JD, Söderberg PG, Bergmanson JP. Lamellar changes in the keratoconic
472   cornea. Acta ophthalmologica. 2015;93(8):767-73.
473   45.   Gefen A, Shalom R, Elad D, Mandel Y. Biomechanical analysis of the keratoconic cornea.
474   Journal of the Mechanical Behavior of Biomedical Materials. 2009;2(3):224-36.

475